Inorganic Chemistry

Article

pubs.acs.org/IC

Heteroleptic (2-Fluoro-3-pyridyl)arylborinic 8-Oxyquinolinates for the Potential Application in Organic Light-Emitting Devices

Grzegorz Wesela-Bauman,*[†,‡] Paulina Ciećwierz,[†] Krzysztof Durka,[†] Sergiusz Luliński,*[†] Janusz Serwatowski,[†] and Krzysztof Woźniak[‡]

[†]Physical Chemistry Department, Faculty of Chemistry, Warsaw University of Technology, Noakowskiego 3, 00-664 Warsaw, Poland

[‡]Laboratory of Crystallochemistry, Department of Chemistry, University of Warsaw, Pasteura 1, 02-093 Warsaw, Poland

Supporting Information

ABSTRACT: A one-pot protocol has been developed to obtain a series of luminescent heteroleptic diarylborinic complexes bearing the 2-fluoro-3-pyridyl and another aryl group attached to the boron atom chelated with a simple or functionalized 8-oxyquinolinato ligand. The tetrahedral geometry around the boron atom in all compounds has been established by the ^{11}B NMR spectroscopy and/or X-ray diffraction technique. In the solution, the obtained complexes have emission maxima ranging from 502 to 525 nm at room temperature. The quantum yield of emission significantly depends on the type and position of the substituents in the 8-oxyquinolinato ligands and aryl rings. An interpretation of the experimental UV−vis absorption and emission spectral data is supported by theoretical calculations of the frontier molecular orbitals. Marcus theory was used to theoretically evaluate charge-transport properties of the obtained complexes.

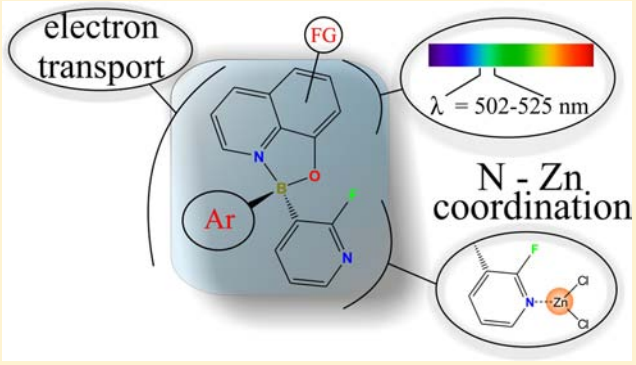

INTRODUCTION

Organoboron complexes are important candidates for the application in light-emitting devices as bright emissive components.[1−7] The first organoboron complexes R_2BQ with an 8-oxyquinolinato (Q) ligand were obtained and characterized by Letsinger and Skoog in 1955.[8] Since then, the chemistry of borinic derivatives has been vigorously developed. This is because they have become a good alternative to the well-known fluorescent aluminum complexes used in the organic light-emitting devices (OLEDs).[9] However, the good luminescent parameters of aluminum complexes are counterbalanced by their limited stability.[10,11] For instance, it was proven by Wang et al.[12−15] that aluminum 7-azaindole complexes are less stable than their corresponding boron counterparts. Furthermore, comparative studies showed that selected boron 8-oxyquinolinates are more efficient emitters than analogous aluminum complexes.[16,17]

Synthetic developments of new luminescent borinic systems are focused mainly on adjusting the wavelength of emission and improving the emission efficiency as well as the stability of these compounds.[1−4,18−22] Chemical functionalization of 8-hydroxyquinoline, especially at the 5 and 7 positions, allows for tuning of the emission color. In most cases, this is responsible for a decrease in the quantum yield (QY) with respect to the reference compound $[Ph]_2B[Q]$, where QY = 23−30%.[23−25] Systematic studies revealed that there are only two known exceptions from this rule, namely, compounds bearing 2-methyl-8-oxyquinolinato (2-Me-Q) and 5-(pinacolatoboron)-8-oxyquinolinate (5-BPin-Q) ligands,[23−26] where a blue-shifted emission band and a significant increase in the QY was observed (34% and 39%, respectively). On the other hand, it seems that modification of the organic substituents attached to the boron center (e.g., by functionalization of the aromatic rings) solely affects the QYs of emission.[20,23−25,27] However, contrary to detailed examination of functionalized 8-hydroxyquinolines, no systematic studies in this area have been performed, so far. In general, diarylborinic 8-oxyquinolinates possess sufficiently high melting points and are not volatile, which is essential for the fabrication of OLEDs, whereas simple dialkylborinic complexes have not appeared to be promising.[28]

In this contribution, we describe a protocol that provides heteroleptic diarylboron complexes, i.e., those containing two different aryl substituents at the boron atom because their chemistry is less explored in comparison with homoleptic analogues.[29] Specifically, our objective was to synthesize complexes bearing at least one heteroaromatic 2-fluoro-3-pyridyl (py) moiety. It should be noted that many nitrogen-based compounds (e.g., aromatic amines, imines, and amides) are commonly used as charge-transport materials in OLEDs.[30] Hence, we assumed that switching from phenyl to py could boost the charge-transport properties of luminescent borinic systems.[31] Experimental results have been supported by

Received: March 25, 2013
Published: September 26, 2013

 © 2013 American Chemical Society dx.doi.org/10.1021/ic400729t | Inorg. Chem. 2013, 52, 10846−10859

Table 1. Synthesis of Diarylborinic Complexes 1−16[a]

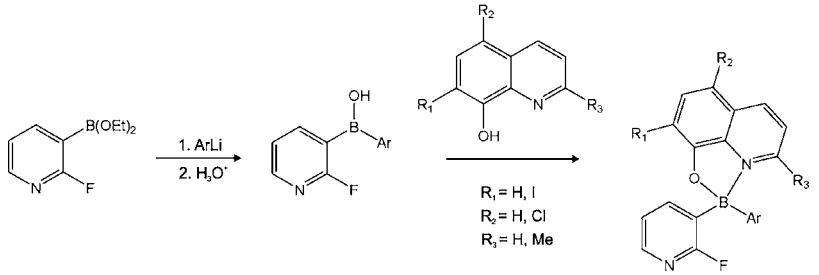

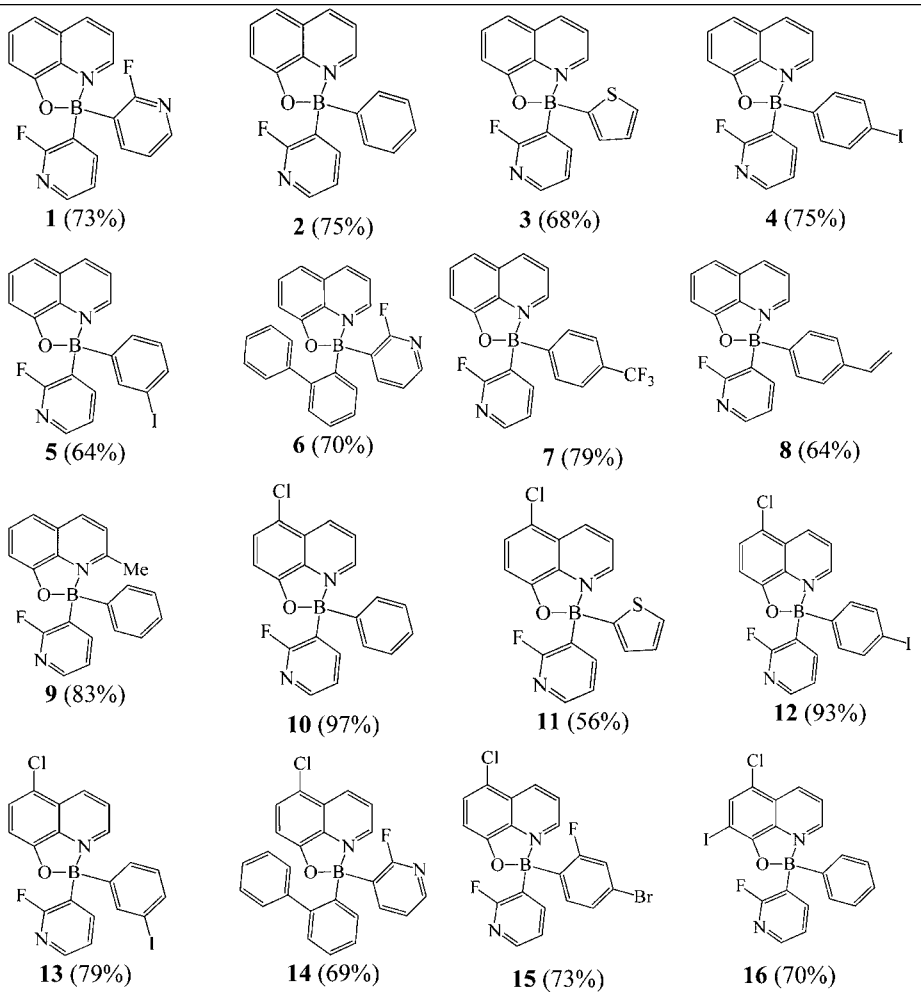

[a]The yields of the isolated products are given in parentheses.

theoretical calculations in order to rationalize the observed optical properties.

In addition, an interesting phenomenon is observed for some borinic complexes with the iodine atom attached to phenyl rings. According to Lakowicz,[32] compounds containing heavy halogens should have their emission quenched because of the formation of an excited triplet state from which molecules can undergo a nonradiative relaxation. Surprisingly, a few examples of iodinated borinic complexes featuring very strong emission (QY = 36−64%) were reported.[22] Therefore, we have also investigated the influence of the iodo substituent on the properties of our systems.

Finally, we were interested in the evaluation of the potential of the synthesized pyridylborinic systems as luminescent ligands able to coordinate to metal centers. Thus, we have studied the complexation of $ZnCl_2$ with selected pyridylborinic systems. The structure and optical properties of the resulting complexes were investigated.

RESULTS AND DISCUSSION

Synthesis of Heteroleptic (2-Fluoro-3-pyridyl)-arylborinic 8-Oxyquinolinates. The key step involves the reaction of 2-fluoro-3-pyridineboronic diethyl ester (**A**) with an appropriate aryllithium at −78 °C in tetrahydrofuran (THF). The resultant diarylborinic "ate" complex of the general formula [py][Ar]B[OEt]$_2$Li is then carefully hydrolyzed with aqueous H_2SO_4 to give the free diarylborinic acid **B**, which is immediately treated with an appropriate H-Q to give a crystalline colorful final product, **1**−**16**. The results are collected in Table 1. This general approach proved problematic

dx.doi.org/10.1021/ic400729t | Inorg. Chem. 2013, 52, 10846−10859

in the synthesis of homoleptic bis(2-fluoro-3-pyridyl)borinic complex **1**. We realized that in this case the free borinic acid is unstable; presumably, it is prone to rapid hydrolysis. The problem was overcome by the addition of H-Q prior to hydrolysis, which gave the fairly stable complex **1**. Unfortunately, we were unable to synthesize analogues of **1** by employing substituted Q ligands. We suppose that a low solubility of the functionalized 8-hydroxyquinolines significantly decreases the rate of complexation, and thus a significant decomposition of bis(2-fluoro-3-pyridyl)borinic acid occurs prior to the formation of a desired product. After complexation with Q, the obtained diarylborinic compounds present an excellent long-term stability in the solid state. It should be stressed that some of them can be used for further transformations because of the presence of reactive functional groups attached to the aryl ring. For instance, the vinyl derivative **8** is a potential monomer for oligo- or polymerization, whereas the iodo derivatives **4**−**5** and **12**−**13** could be used in coupling reactions.

Complexation of $ZnCl_2$ with Selected Azaesters. Currently, the chemistry of zinc pyridine complexes is rapidly expanding.[33−41] Recently, Jäkle and co-workers reported that complexation of a borinic polymeric system bearing attached pyridine moieties with zinc tetraphenylporphyrin changed the wavelength of emission.[42] This has prompted us to investigate the formation of complexes between our compounds and $ZnCl_2$. For compounds **2**−**16** bearing one py group, one can expect the formation of two types of complexes depending on the zinc/ligand ratio ($ZnCl_2L$ or $ZnCl_2L_2$). In the case of bis(pyridyl) ligand **1**, oligomers or even coordination polymers can potentially be formed. We have prepared complexes of the type $ZnCl_2L_2$, where L = **2**, **10**, and **12**, by the addition of $ZnCl_2$ to the ligand (in a ratio of 1:2) dissolved in CH_2Cl_2. The respective products **17**−**19** were isolated by precipitation with hexane as yellow or greenish solids in good yields. We have confirmed the assumed composition for all obtained complexes by elemental analysis. We have also compared their ^{1}H NMR spectra with those recorded for free ligands (Figure 1). They show that there is a low-field shift of signals attributed to the py moiety in the zinc complexes (up to ca. 0.5 ppm), which suggests a charge depletion within the heterocycle due to the formation of Zn−N dative bonds. On the other hand, the ^{11}B NMR spectra remain essentially unchanged in accordance with the weak effect of the complex formation on the boron atom environment. Specifically, this indicates that the potential translocation of the 8-oxyquinolinato ligand from boron to zinc does not occur to any extent. In addition, we have found that mixing equimolar amounts of $ZnCl_2$ and **1** resulted in the precipitation of a yellow solid from the CH_2Cl_2 solution. Elemental analysis revealed that the approximate composition of this material can be given as $3[ZnCl_2]\cdot 2[\mathbf{1}]$. However, the product was not completely soluble in $CDCl_3$, and the slow evaporation of the resulting solution in the NMR tube gave a few single crystals of the dinuclear zinc complex $\{ZnCl_2[\mathbf{1}]\}_2$ (**20**). We are planning to extend these studies toward the synthesis of complexes with other metal centers.

Crystal Structure Analysis. The crystal structures of **1**, **3**, **4**, and **10** have been determined by using single-crystal X-ray diffraction. In addition, the complexes of $ZnCl_2$ with **1** and **2** have also been crystallographically characterized (**20** and **17**, respectively). Single crystals were obtained by a slow evaporation of acetone (for **1** and **3**) or CH_2Cl_2 (for **4** and **10**) solutions. As expected on the basis of ^{11}B NMR spectra, all

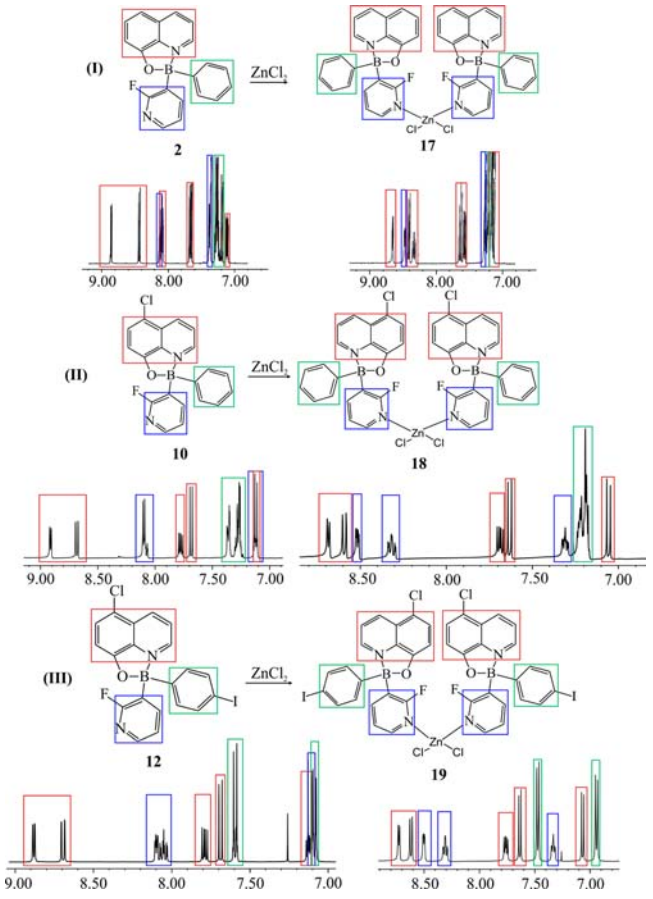

Figure 1. Complexation of $ZnCl_2$ with selected borinic ester ligands illustrated by changes in the ^{1}H NMR spectra (400 MHz, $CDCl_3$).

compounds display a typical tetrahedral geometry, with Q chelating the boron atom to form the five-membered ring. Details of data collection and structure refinement are summarized in Table 2. Selected bond lengths and angles are listed in Table 3.

The molecular structures of **1**, **3**, **4**, and **10** are depicted in Figure 2. Parameters that describe the geometry of the boron coordination sphere, both the bond lengths and valence angles, do not significantly differ within the studied compounds. The values of the tetrahedral character (THC) parameter[43] (Table 3) proved that the deviation from ideal tetrahedral geometry is similar for all crystal structures. The crystal packing in **1**, **3**, **4**, and **10** is dominated by weak interactions, including mainly C−H···O, C−H···π, and $\pi\cdots\pi$ contacts (Figure 3). Their distribution was characterized by Hirshfeld surface[44−47] analyses (Figure S2 in the Supporting Information).

In the case of **17**, single crystals suitable for X-ray analysis were obtained by slow evaporation of the solution in a mixed solvent (acetone/toluene, ca. 1:1). The X-ray structure of **17** shows that the geometry around the zinc coordination center is similar to that observed in related complexes of $ZnCl_2$ with two pyridine ligands.[48−52] It should be noted that there is a possibility for the formation of two diastereomers of **17** because of ligand chirality. However, the crystal structure of **17** comprises homochiral enantiomeric molecules (*R*,*R* and *S*,*S*) related by the center of symmetry (Figure 4). The metric parameters of the bound ligand **2** (Table 4) are comparable to those found for structurally characterized free ligands described above. X-ray analysis of **20** revealed a dimeric macrocyclic

dx.doi.org/10.1021/ic400729t | *Inorg. Chem.* 2013, 52, 10846−10859

Table 2. Selected Crystal Data and Refinement Details for Compounds 1, 3, 4, 10, 17, and 20

	1	3	4	10
chemical formula	$C_{19}H_{12}BF_2N_3O$	$C_{18}H_{12}BFN_2OS$	$C_{20}H_{13}BFIN_2O$	$C_{20}H_{13}BClFN_2O$
M_r	347.13	334.17	454.03	362.58
space group	$P2_1/n$	$P2_1/c$	$P2_1/n$	$Pna2_1$
cell settings: a, b, c (Å)	6.9910(6), 12.7231(12), 17.5105(15)	9.5208(3), 14.3566(4), 12.1658(4)	6.8035(2), 14.6623(3), 17.1152(4)	6.0002(7), 22.295(3), 12.1967(13)
α, β, γ (deg)	90.000, 91.999(8), 90.000	90.000, 109.901(4), 90.000	90.000, 90.967(2), 90.000	90.000, 90.000, 90.000
V (Å^3)	1556.6(2)	1563.59(8)	1707.08(7)	1631.6(3)
Z	4	4	4	4
d (Mg m^{-3})	1.481	1.420	1.767	1.476
no. of measd, indep, and obsd [$F^2 > 2\sigma(F^2)$]	18466, 4717, 2147	54028, 3074, 2608	30788, 4171, 3575	9273, 2959, 1637
R_{int} (%)	6.4	5.1	2.4	8.8
θ_{max} (deg)	30.51	26.02	28.72	25.68
R1 [$F^2 > 2\sigma(F^2)$], wR2 (F^2), GOF	0.0343, 0.0494, 0.705	0.0774, 0.1905, 1.102	0.0185, 0.0438, 1.069	0.0402, 0.0673, 1.000
no. of param	235	224	235	235
$\Delta\rho_{max}$, $\Delta\rho_{min}$ (e Å^{-3})	0.22, −0.19	1.44, −0.79	0.51, −0.45	0.70, −0.65

	17	20
chemical formula	$2C_{40}H_{28}B_2Cl_2F_2N_4O_2Zn\cdot H_2O$	$2C_{38}H_{24}B_2Cl_4F_4N_6O_2Zn_2\cdot 3CDCl_3$
M_r	1603.16	2294.77
space group	$Pbcn$	$P\bar{1}$
cell settings: a, b, c (Å)	14.281(1), 8.148(1), 31.200(1)	9.553(1), 11.982(1), 24.289(1)
α, β, γ (deg)	90.00, 90.00, 90.00	91.79(1), 97.60(1), 104.20(1)
V (Å^3)	3630.6(1)	2665.9(2)
Z	2	1
d (Mg m^{-3})	1.466	1.429
no. of measd, indep, and obsd [$F^2 > 2\sigma(F^2)$]	93231, 6456, 4835	49567, 11988, 6532
R_{int} (%)	8.3	11.5
θ_{max} (deg)	32.56	32.64
R1 [$F^2 > 2\sigma(F^2)$], wR2 (F^2), GOF	0.047, 0.102, 1.10	0.115, 0.351, 1.04
no. of param	245	631
$\Delta\rho_{max}$, $\Delta\rho_{min}$ (e Å^{-3})	0.48, −0.37	2.02, −0.78

Table 3. Selected Bond Lengths (Å) and Angles (deg) for 1, 3, 4, and 10[a]

	1	3[b]	4	10
B(1)−O(1)	1.517(2), *1.521*	1.519(6), *1.519/1.518*	1.513(2), *1.521*	1.542(7), *1.521*
B(1)−N(1)	1.627(2), *1.646*	1.622(5), *1.651/1.651*	1.630(2), *1.661*	1.610(7), *1.656*
B(1)−C(Ar)	1.609(2), *1.616*	1.552(6), *1.604/1.607*	1.609(2), *1.613*	1.595(8), *1.614*
B(1)−C(py)	1.606(2), *1.617*	1.614(6), *1.619/1.618*	1.613(2), *1.623*	1.623(8), *1.619*
C(py)−B(1)−C(Ar)	114.2(1), *116.1*	115.0(4), *115.6/116.6*	114.6(1), *117.4*	114.1(4), *116.1*
C(Ar)−B(1)−O(1)	110.7(1), *109.7*	111.2(3), *111.2/109.3*	109.6(1), *110.9*	110.9(4), *111.4*
O(1)−B(1)−N(1)	99.43(9), *98.8*	99.6(3), *98.4/98.7*	99.5(1), *98.1*	98.7(4), *98.3*
N(1)−B(1)−C(py)	111.2(1), *110.3*	111.2(3), *110.9/110.9*	113.8(1), *110.9*	108.1(4), *110.8*
C(py)−B(1)−O(1)	109.8(1), *110.1*	109.2(3), *111.2/111.1*	108.7(1), *108.2*	110.8(4), *110.5*
N(1)−B(1)−C(Ar)	110.6(1), *110.5*	109.6(3), *108.4/108.8*	109.4(1), *109.7*	113.1(4), *108.3*
THC	80(2), *77*	78(6), *70/73*	86(2), *75*	77(7), *70*

[a]Theoretical values obtained at the RB3LYP/6-31+g(d,p) level of theory are presented in italics. [b]Two sets of values calculated for two rotamers **3A**/**3B** with two opposite positions of thienyl ring.

structure where **1** acts as a ditopic ligand for two zinc atoms. A few related macrocycles have been reported.[53−58] The geometry around the zinc atom is similar to that found for **17**. In both complexes, the crystal packing is based mainly on weak C−H···π and π-stacking interactions, which occurred between two neighboring quinoline moieties, with interplanar separation distances equal to 3.360(6) Å (**17**) and 3.567(4) Å (**20**).

Optical Properties. The optical properties of **1**−**19** were investigated by UV−vis absorption and photoluminescence spectroscopy in THF or CH_2Cl_2 solutions at ambient conditions (Figure 5a−c). The photophysical data for model compounds [Ph]$_2$B[Q] and [Ph]$_2$B[2-Me-Q] and **1**−**19** are summarized in Table 5. The experimental results were complemented by theoretical (time-dependent density functional theory, TD-DFT) calculations. They were performed separately for two rotamers of **3** and **11** with two opposite positions of the 2-thienyl (Th) ring similar to those observed in the disordered crystal structure of **3**.

Compounds **1**−**8** exhibit absorption maxima in the range 381−390 nm, arising from the Q chromophors.[59] These bands exhibit a hypsochromic shift relative to [Ph]$_2$B[Q] (396 mm). A slightly stronger blue shift is observed for the 2-Me-Q complex **9** (378 nm). Conversely, a bathochromic shift is

dx.doi.org/10.1021/ic400729t | *Inorg. Chem.* 2013, 52, 10846−10859

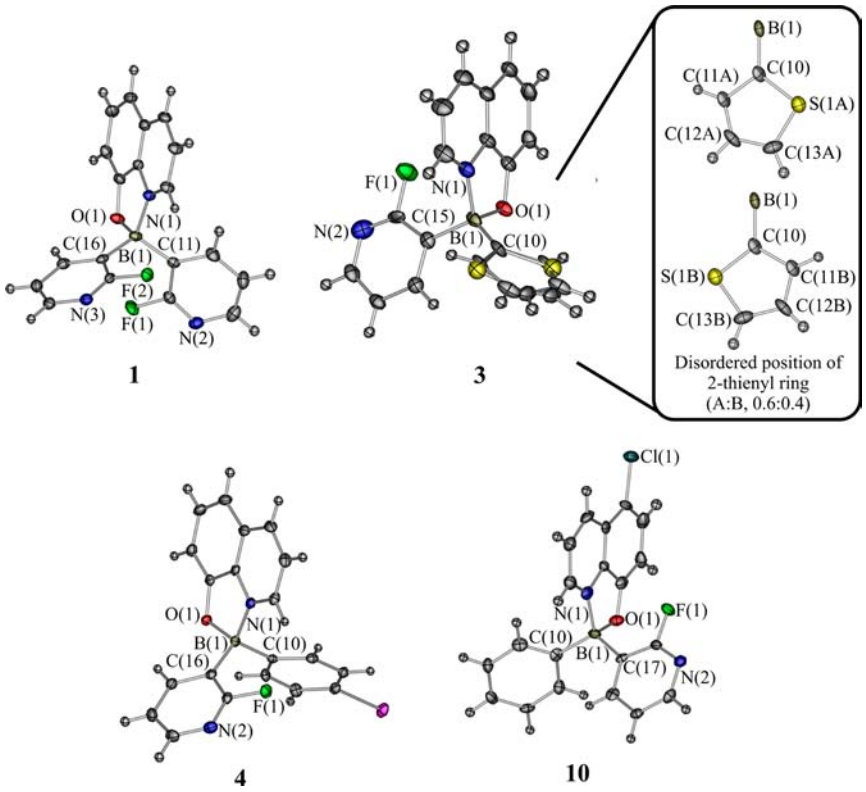

Figure 2. Molecular structures of **1**, **3**, **4**, and **10** with atom-labeling schemes. Thermal ellipsoids were generated at the 50% level of probability.

observed for compounds bearing 5-Cl-Q and 5-Cl-7-I-Q ligands. The emission data for all compounds were obtained after excitation at the longest-wavelength absorption band. One maximum of emission is observed for all compounds. There is no correlation between the bond lengths derived from the crystal structures (or from geometry optimization) and the observed λ_{em} values. It is clear that functional groups attached to the boron atom do not influence the maxima of emission, which is in agreement with previous results.[1−4]

All compounds (except for zinc complexes) are medium-intense emitters with QY up to 20%. Functionalization of Q resulted in lower QY values. However, the synthesized 5-Cl-Q complexes (**10**−**16**) have higher QYs with respect to the related complex synthesized by Jäkle et al.[26] (QY = 8%). The effect of iodine was position-dependent because *m*-iodophenyl derivatives have their QYs higher than the para-substituted analogues (for both Q and 5-Cl-Q; Table 5). It is known[1−4] that the highest occupied molecular orbitals (HOMOs) span across the phenolate ring and the lowest unoccupied molecular orbitals (LUMOs) across the pyridine ring of the Q ligand. Thus, introduction of an electron-withdrawing substituent into the 5 and 7 positions of Q should result in a lowering of the HOMO level. As a consequence of a greater HOMO−LUMO energy gap, a blue shift in the absorption and emission spectra should be found. However, the complexes with 5-Cl-Q and 5-Cl-7-I-Q (**10**−**16**) exhibit a red shift in the obtained spectra, which indicates that the electron-withdrawing inductive effect of halogen on the Q moiety is weaker than the mesomeric donation of the electron density. On the other hand, the electron-donating group in the second position of the Q ligand should decrease the LUMO energy level, resulting in a red shift. This is not confirmed by the absorption and emission spectra of **9**, where a slight blue shift is observed. Zinc complexes **17**−**19** exhibit absorption at a slightly longer wavelength with respect to the free ligands **2**, **10**, and **12**. On the other hand, the wavelength of emission was not affected by formation of the Zn−N dative bond. However, it should be stressed that the QYs of emission were decreased to 2−3%. This indicates that complexation with $ZnCl_2$ opens new effective pathways for nonradiative relaxation.

Electrochemical Properties. We have performed cyclic voltammetry (CV) studies of selected compounds (**1** and **3**−**5**) in order to establish their electrochemical redox properties in an organic solvent (CH_3CN). Potentials were assigned versus the ferrocene−ferrocenium ($FeCp_2/FeCp_2^+$) redox couple (Table 6). The recorded CV curves are shown in Figure 6. All of them show irreversible oxidation and reduction. Scanning at a faster scan rate did not improve the reversibility of the redox processes. The irreversible nature of the oxidation of these compounds could be caused by the electron-deficient py ring, which destabilizes the oxidized forms of the analyzed compounds. Compound **1** shows one oxidation peak, whereas two oxidation peaks can be distinguished for compounds **3**−**5**. For the latter compounds, the HOMO energies were calculated based on the lower oxidation potentials. Thus, the obtained values are −6.09 eV for **1** and −5.99 eV for **3**−**5**. These values are slightly lower than the one reported for $[Ph]_2B[Q]$ (−5.8 eV).[60] We suppose that this effect can be attributed mainly to the presence of a py substituent and can be compared to the lowering of the HOMO in the perfluoro compound $[C_6F_5]_2B[Q]$ (−5.9 eV).[60]

Molecular Orbital Calculations. In order to establish the precise electronic structure of the synthesized compounds and the nature of the orbitals involved in the electronic transitions, we have performed geometry optimization of isolated molecules using DFT methods at the B3LYP/6-31+g(d,p)

dx.doi.org/10.1021/ic400729t | *Inorg. Chem.* 2013, 52, 10846−10859

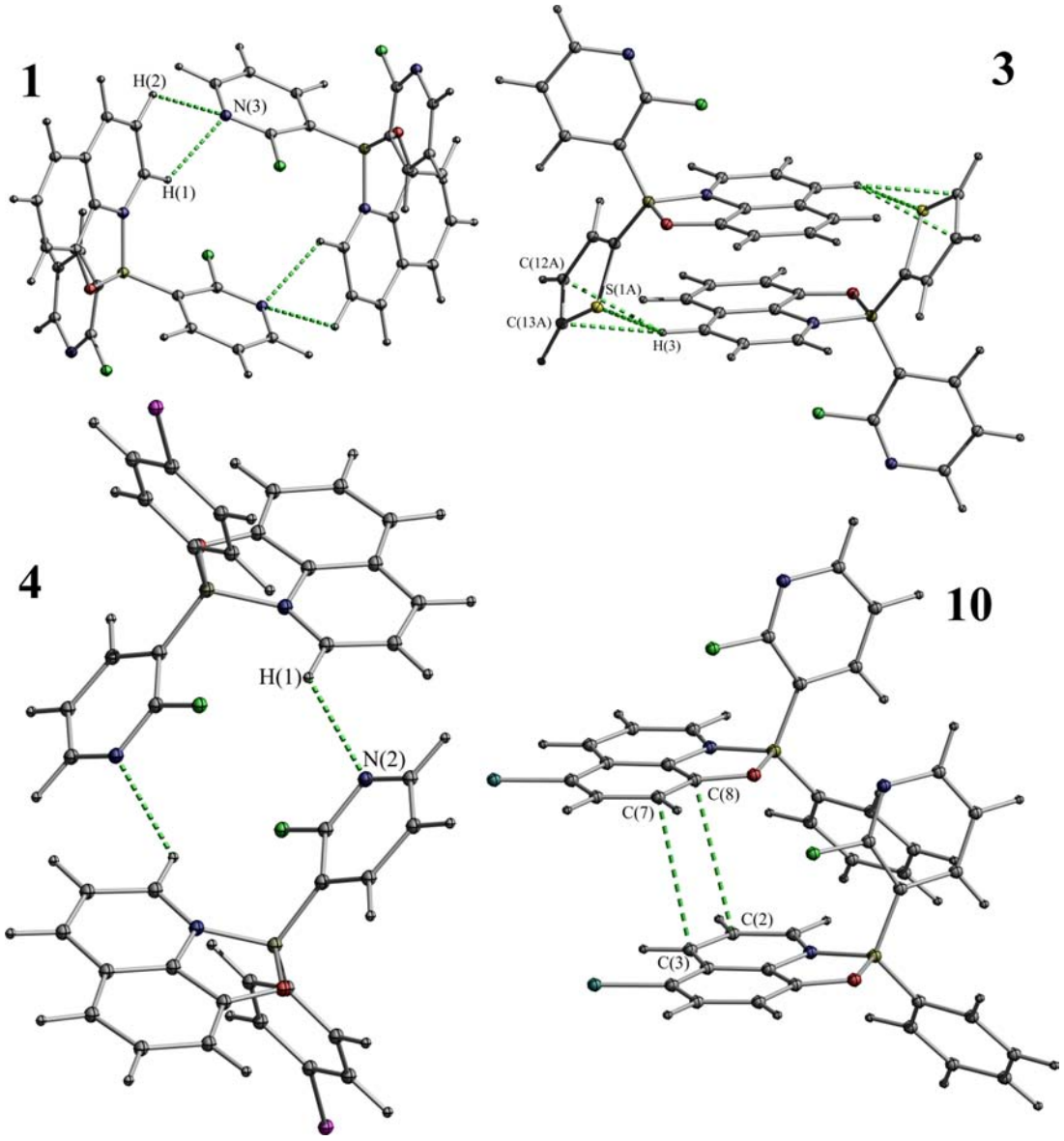

Figure 3. Crystal packing motifs for compounds **1**, **3A**, **4**, and **10**.

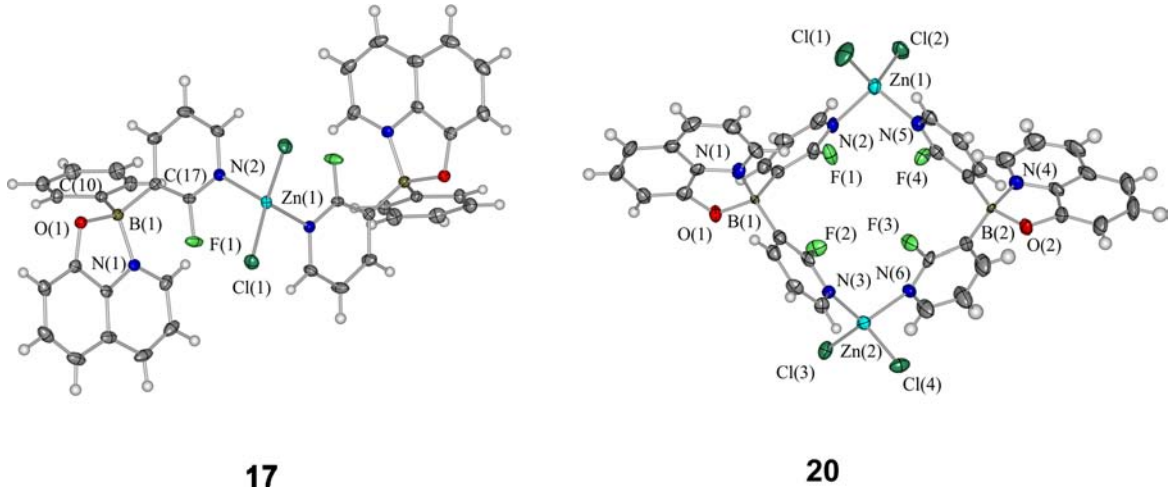

17 **20**

Figure 4. Molecular structures of the complexes of $ZnCl_2$ with **2** (**17**) and **1** (**20**) together with atom-labeling schemes. Thermal ellipsoids were generated at the 50% level of probability. Solvent molecules incorporated into the structures are omitted for clarity.

dx.doi.org/10.1021/ic400729t | *Inorg. Chem.* 2013, 52, 10846−10859

Table 4. Selected Bond Lengths (Å) for 17 and 20

17		20			
B(1)−O(1)	1.514(2)	B(1)−O(1)	1.51(1)	B(2)−O(2)	1.49(1)
B(1)−N(1)	1.616(2)	B(1)−N(1)	1.62(1)	B(2)−N(4)	1.63(1)
B(1)−C(Ar)	1.613(2)	B(1)−C(10)	1.61(1)	B(2)−C(29)	1.62(1)
B(1)−C(py)	1.628(2)	B(1)−C(15)	1.63(1)	B(1)−C(34)	1.63(1)
Zn(1)−N(2)	2.075(1)	Zn(1)−N(2)	2.048(7)	Zn(2)−N(3)	2.043(8)
		Zn(1)−N(6)	2.069(6)	Zn(2)−N(5)	2.073(7)
Zn(1)−Cl(1)	2.230(4)	Zn(1)−Cl(1)	2.215(3)	Zn(2)−Cl(3)	2.216(3)
		Zn(1)−Cl(2)	2.216(3)	Zn(2)−Cl(4)	2.214(3)

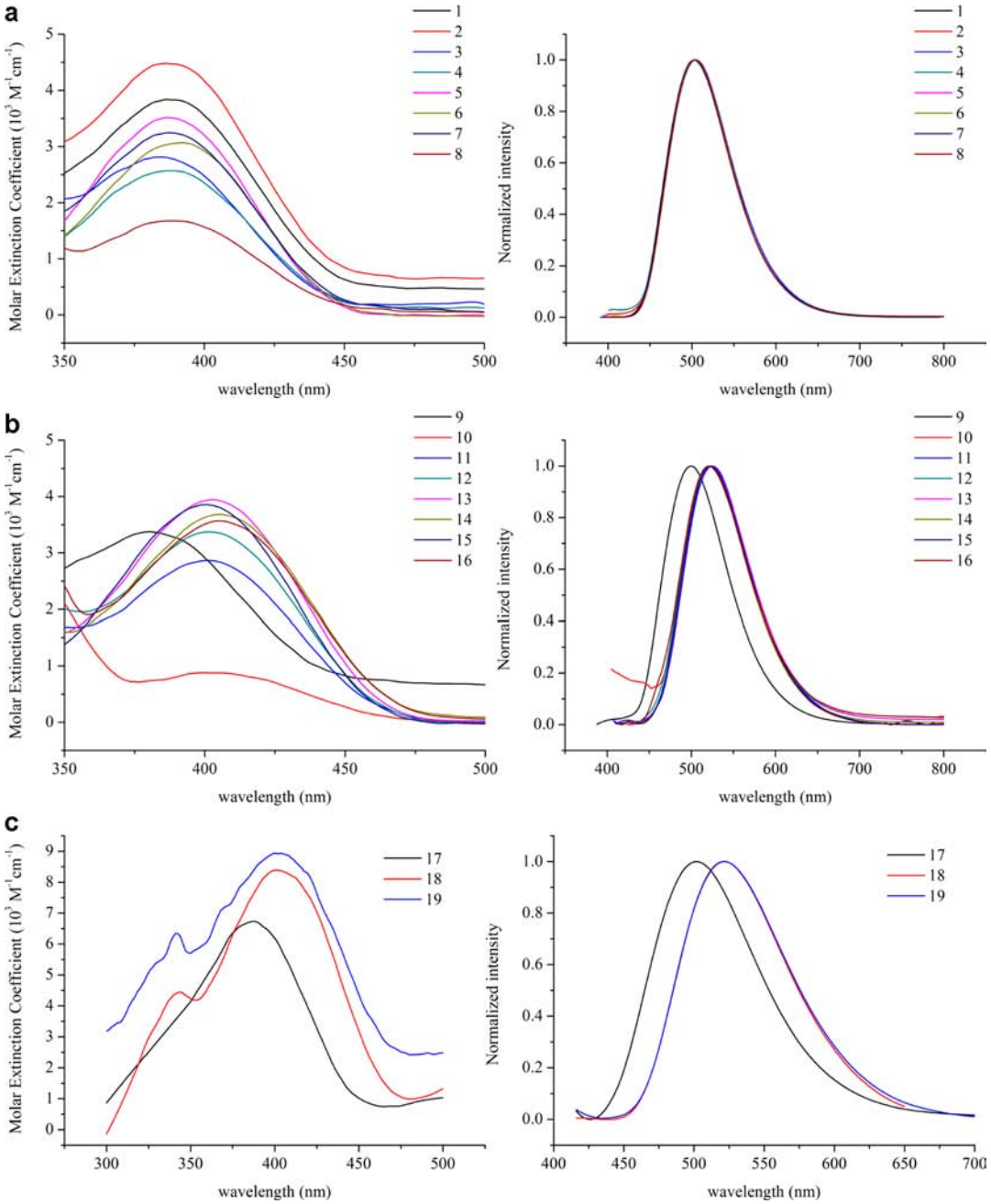

Figure 5. UV−vis absorption (left) and fluorescence (right) spectra of (a) **1**−**8** in THF, (b) **9**−**16** in THF, and (c) **17**−**19** in CH_2Cl_2.

level of theory for both the ground state and the first singlet excited state (TD-DFT).[61−63] According to the calculations, vertical excitations for these compounds are observed predominantly because of the HOMO → LUMO (**1**−**2**, **6**−**7**, **9**−**10**, **14**, and **16**) or simultaneously HOMO and HOMO−1 → LUMO transitions (**3**−**5** and **12**−**13**). The pure HOMO−1 → LUMO excitations are observed for **8**, **11**, and **15**. All observed excitations correspond to $\pi-\pi^*$ transitions. For all

dx.doi.org/10.1021/ic400729t | *Inorg. Chem.* 2013, 52, 10846−10859

Table 5. Experimental and Calculated Photophysical Properties

		experimental data				TD-DFT	
	compound	λ_{max} [nm]	ε [M^{-1} cm^{-1}]	λ_{em} [nm]	Φ [%][b]	λ_{max} [nm][e]	λ_{em}[nm][e]
	$[Ph]_2B[Q]$[f]	396		504	30[c]/23[d]	416 (n/a)	516 (n/a)
	$[Ph]_2B$[2-Me-Q][f]	396		497	34[c]		
1	$[py]_2B[Q]$[a]	381	3800	502	18	430 (0.057)	567 (0.036)
2	[Ph][py]B[Q][a]	384	4400	503	20	422 (0.054)	561 (0.038)
3	[Th][py]B[Q][a]	382	2800	504	20	425 (0.051)/425 (0.050)	589 (0.032)/591 (0.030)
4	[4-I-Ph][py]B[Q][a]	391	2600	504	15	419 (0.037)	561 (0.039)
5	[3-I-Ph][py]B[Q][a]	390	3500	503	18	417 (0.058)	561 (0.036)
6	[2-Ph-Ph][py]B[Q][a]	390	3100	504	16	421 (0.043)	551 (0.031)
7	[4-CF_3-Ph][py]B[Q][a]	388	3300	503	16	416 (0.060)	562 (0.038)
8	[4-vinyl-Ph][py]B[Q][a]	390	1700	504	14	415 (0.071)	489 (0.086)
9	[Ph][py]B[2-Me-Q][a]	378	3300	500	20	434 (0.043)	580 (0.029)
10	[Ph][py]B[5-Cl-Q][a]	395	870	522	10	448 (0.067)	628 (0.038)
11	[Th][py]B[5-Cl-Q][a]	397	2900	525	11	446 (0.061)/446 (0.062)	603 (0.039)/633 (0.035)
12	[4-I-Ph][py]B[5-Cl-Q][a]	399	3400	521	14	440 (0.052)	602 (0.045)
13	[3-I-Ph][py]B[5-Cl-Q][a]	401	4000	523	18	438 (0.069)	602 (0.041)
14	[2-Ph-Ph][py]B[5-Cl-Q][a]	407	3700	522	12	441 (0.055)	589 (0.037)
15	[4-Br-2-F-Ph][py]B[5-Cl-Q][a]	399	3900	523	18	415 (0.071)	601 (0.042)
16	[Ph][py]B[5-Cl-7-I-Q][a]	405	3700	520	19	449 (0.057)	608 (0.037)
17	$ZnCl_2$·[**2**]$_2$[c]	389	6700	502	3	n/a	n/a
18	$ZnCl_2$·[**10**]$_2$[c]	404	8300	522	3	n/a	n/a
19	$ZnCl_2$·[**12**]$_2$[c]	406	8900	521	2	n/a	n/a

[a]Measured in THF. [b]Relative to DPA in cyclohexane at room temperature. Excited at the longest-wavelength absorption band. [c]Measured in CH_2Cl_2. [d]Measured in $CHCl_3$. [e]The values of the oscillator strength (f) are given in parentheses. [f]Data taken from refs 23−25.

Table 6. Electrochemical Data and Calculated HOMO−LUMO Energies for Compounds 1 and 3−5

compound	E_{ox} [V][a]	E_{red} [V][a]	HOMO [eV]	LUMO [eV]	energy gap [eV]
1	1.290	−1.724	−6.09	−3.08	3.01
3	1.195, 1.310	−1.735	−5.99	−3.06	2.93
4	1.194, 1.296	−1.730	−5.99	−3.07	2.92
5	1.192, 1.304	−1.724	−5.99	−3.08	2.91

[a]Values calculated on the basis of the peak potentials and given with respect to the $FeCp_2/FeCp_2^+$ redox pair.

compounds, the py moiety does not contribute significantly to either the HOMO or LUMO, although it may contribute to HOMO−1. Distribution of the frontier orbitals for **1** and **2** (Figure 7) is representative for the entire series of complexes. The complete listing of generated orbitals and their energies for **1**−**16** is provided in the Supporting Information (Tables S4 and S5).

Visualization of the orbital energies for **1**−**16** has been shown in Figure 8. We have found that the HOMO−LUMO gap is decreased by attaching functional groups such as 5-Cl and 5-Cl-7-I to the Q ligand, which is consistent with bathochromic shifts observed in the experimental spectra. Theoretical calculations for **9** predict a narrowing of the HOMO−LUMO band gap, which is in contradiction with an observed blue-shifted absorption. It seems that the energy gap can be further tuned by functional groups introduced onto an aryl group attached to the boron atom. Compounds **4** and **12** with the *p*-iodophenyl group have their HOMO levels higher

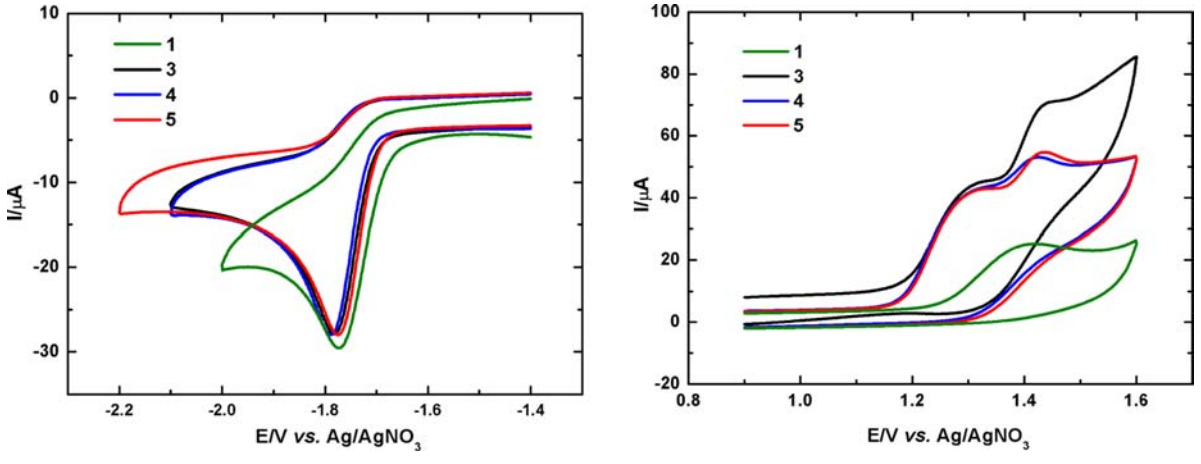

Figure 6. Cyclic voltammograms of **1** and **3**−**5** (1 mM) in 0.1 M Bu_4NPF_6/CH_3CN. ν = 0.1 V s^{-1}.

dx.doi.org/10.1021/ic400729t | Inorg. Chem. 2013, 52, 10846−10859

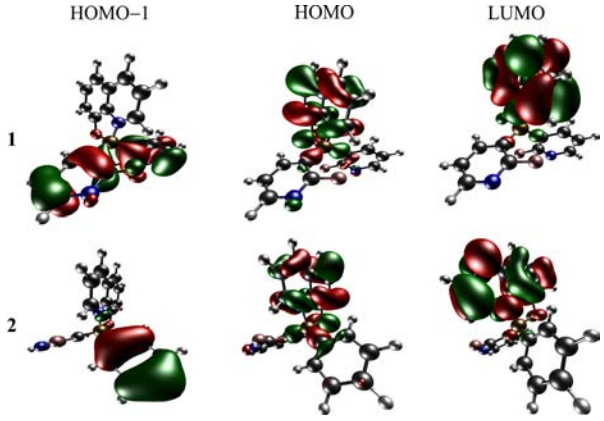

Figure 7. Plots of the HOMO−1, HOMO, and LUMO levels of compounds **1** and **2** (contour 0.03 e Å^{-3}).

than the corresponding *m*-iodo derivatives **5** and **13**, while LUMO energies remain essentially unchanged. This can be rationalized by the weaker electron-withdrawing effect of the *p*-iodo derivative. However, a comparison of the QY values measured for our compounds (Table 5) does not allow one to draw strong conclusions regarding the correlation of the optical properties with the electronic effects of iodine.

Charge-Transport Properties. The charge-transport properties of **1**−**16** were evaluated using Marcus theory.[64] Because the recombination of holes and electrons takes place in the emitting layer of OLEDs, the compounds that create emitting layers should have balance between the hole injections and electron acceptance. Hence, the most promising and efficient emitters should have low values of electron and hole reorganization energies ($\Lambda_{electron}$ and Λ_{hole}), and these energies should be similar. The values calculated for **1**−**16** (Table 7) indicate that, from the standpoint of the reorganization energy, the studied compounds could act as hole-transport materials.

Table 7. Reorganization Energies (eV) for 1−16

	compound	Λ_{hole}	$\Lambda_{electron}$	$\lvert\Delta\Lambda\rvert$
	Al[Q]$_3$[a]	0.24	0.28	0.04
1	[py]$_2$B[Q]	0.22	0.41	0.19
2	[Ph][py]B[Q]	0.23	0.45	0.22
3A	[Th][py]B[Q]	0.37	0.41	0.03
3B		0.20	0.46	0.26
4	[4-I-Ph][py]B[Q]	0.24	0.42	0.18
5	[3-I-Ph][py]B[Q]	0.13	0.47	0.34
6	[2-Ph-Ph][py)B[Q]	0.25	0.42	0.17
7	[4-CF$_3$-Ph][py]B[Q]	0.26	0.42	0.16
8	[4-vinyl-Ph][py]B[Q]	0.29	0.42	0.13
9	[Ph][py]B[2-Me-Q]	0.21	0.40	0.19
10	[Ph][py]B[5-Cl-Q]	0.29	0.40	0.10
11A	[Th][py]B[5-Cl-Q]	0.38	0.41	0.03
11B		0.34	0.46	0.12
12	[4-I-Ph][py]B[5-Cl-Q]	0.24	0.42	0.18
13	[3-I-Ph][py]B[5-Cl-Q]	0.16	0.44	0.28
14	[2-Ph-Ph][py]B[5-Cl-Q]	0.24	0.42	0.18
15	[4-Br-2-F-Ph][py]B[5-Cl-Q]	0.31	0.39	0.07
16	[Ph][py]B[5-Cl-7-I-Q]	0.27	0.40	0.14

[a]Data taken from ref 65.

The most efficient hole-transport ability (significantly better when compared to Al[Q]$_3$) was predicted for **5** and **13** based on the relatively low values of Λ_{hole}. However, these compounds (bearing 3-I-Ph group) possess relatively high values of $\Lambda_{electron}$. The balanced hole- and electron-transport properties are essential for compounds used in OLEDs. Such a balance is observed for **3A**, **11A**, and **15**. It is not clear what the origin of different reorganization energies of two conformers of **3** and **11** is. This is quite intriguing because molecular orbital calculations proved that both Th and py do not contribute to HOMO and LUMO, although the former contributes significantly to HOMO−1. We suppose that the reorganization

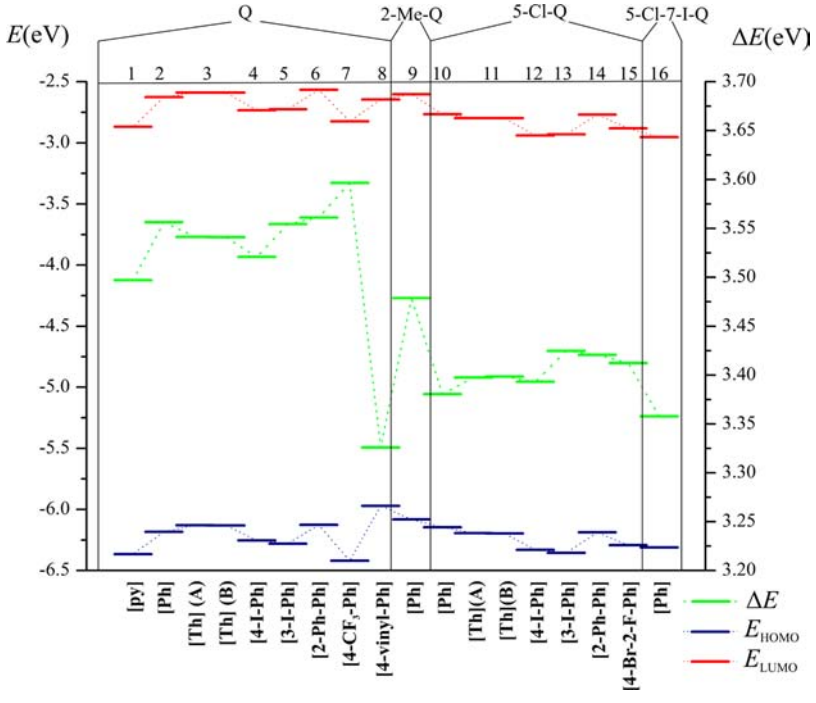

Figure 8. Calculated HOMO and LUMO energies and ΔE values, $\Delta E = E_{LUMO} - E_{HOMO}$.

dx.doi.org/10.1021/ic400729t | *Inorg. Chem.* 2013, 52, 10846−10859

energies in the conformers **3A** and **11A** may be influenced by the interaction between sulfur and oxygen atoms, which is not the case for **3B** and **11B**.

Analysis of the calculated reorganization energies may lead to the conclusion that compounds **1**−**16** are hole-transport materials. It should be noted that comparable results were reported for other borinic 8-oxyquinolinates.[66] This is in contradiction with the experimental evidence for the electron-transport properties of $[Ph]_2B[Q]$.[28] Similarly, theoretical analysis of the charge-transport properties of $Al[Q]_3$ based solely on the reorganization energies indicated that $Al[Q]_3$ should act as a hole-transport material despite experimental evidence of its electron-transport properties. However, additional calculations of the transfer integrals (H_{AB}) for $Al[Q]_3$ resulted in the proper correlation with the experiment. This may be due to the fact that the reorganization energies for our systems and $Al[Q]_3$ were conducted in the gas phase. Thus, we have expanded our research by calculations of the transfer integrals for systems characterized by X-ray diffraction (**1**, **3**, **4**, and **10**). On the basis of the Marcus−Hush two-state model,[67] H_{AB} of a given system can be approximated by the energy splitting of the electronic levels. When two molecules approach to each other, their HOMOs and LUMOs start to interact, and new HOMO/HOMO−1 and LUMO/LUMO+1 are being formed. The energetic splitting for the hole transfer is equal to the half of the energy difference between HOMO and HOMO−1 calculated for the pair of interacting molecules. Similarly, the splitting for the electron transfer is equal to the half of the energy difference between LUMO and LUMO+1 for the pair of interacting molecules. The results obtained with the B3LYP potential are summarized in Table 8. Calculations

Table 8. Total Charge-Transport Integrals (H_{AB}) for Compounds 1, 3, 4, and 10

	H_{AB} (eV)		
compound	hole	electron	charge transport
1	1.39	1.63	electron
3A/3B	1.11/1.09	0.92/0.87	hole
4	0.77	1.15	electron
10	1.34	1.53	electron

proved that crystal lattices of compounds **1**, **4**, and **10** present electron-transport properties, whereas both virtual crystal lattices of **3** composed of either conformer **3A** or **3B** are predicted to be more suitable for hole transport. However, it is possible that this approach is not a good approximation because it does take into account the mutual interactions between disordered **3A** and **3B** conformers in the real crystal lattice.

CONCLUSIONS

In conclusion, we have developed a synthetic approach to a novel class of fluorescent diarylborinic 8-oxyquinolinates bearing at least one py moiety. By changing the substituents attached to the Q ligand, we were able to obtain compounds with the wavelength of emission ranging from 502 to 525 nm and moderate QY values varying in the range 10−20%. In addition, NMR and X-ray diffraction studies point to the formation of complexes with $ZnCl_2$ through the coordination of zinc with the pyridyl nitrogen atom. Further examination of complexes with other metal coordination centers is planned. It is plausible that complexes **1**−**16** could be used as building blocks in the construction of various supramolecular luminescent systems, specifically those based on the formation of a metal−nitrogen dative bond.

There are no simple correlations between the molecular parameters of the boron coordination sphere (in both gas and solid states) and the observed optical properties. On the other hand, theoretical calculations indicate that the energy and distribution of frontier orbitals can be modified by chemical functionalization. The charge-transport properties were evaluated in the framework of Marcus theory. It was demonstrated that calculations limited to gas-phase conditions may give misleading results. Thus, analysis of the interactions in the solid phase proved to be necessary for the more accurate prediction of the charge-transport character of studied systems. The obtained results indicate that the analyzed compounds can be regarded as electron-transport systems. This is also suggested by the electrochemical estimation of the HOMO/LUMO energies for selected compounds, although these results should be interpreted with care because of the lack of reversibility of the redox processes.

EXPERIMENTAL SECTION

Syntheses of 1−19. All reactions involving air- and moisture-sensitive reagents were carried out under an argon atmosphere. Et_2O and THF were stored over a sodium wire before use. Starting materials 2-fluoropyridine, halogenated benzenes, 8-hydroxyquinolines, and other important reagents including *n*-BuLi (10 M in hexanes), diisopropylamine, chlorotrimethylsilane, triethyl borate, and $ZnCl_2$ (1 M in Et_2O) were received from Aldrich and used without further purification. The NMR chemical shifts are given relative to tetramethylsilane $[Si(CH_3)_4]$ by using known chemical shifts of residual proton (^1H) or carbon (^{13}C) solvent resonances. In the ^{13}C NMR spectra of arylborinic complexes, the resonances of boron-bound carbon atoms were not observed in most cases as a result of their broadening by a quadrupolar boron nucleus. ^1H and ^{13}C NMR spectra were recorded on a Varian Mercury 400 MHz spectrometer, and ^{11}B NMR spectra were recorded a Varian Unity Plus 200 MHz spectrometer.

*Synthesis of Diethyl (2-Fluoropyridin-3-yl)boronate (**A**).* To the solution of lithium diisopropylamide (0.1 mol) freshly prepared from diisopropylamine (10.7 g, 0.105 mol) and *n*-BuLi (10 M, 10 mL, 0.1 mol) in THF (100 mL) was added at −78 °C 2-fluoropyridine (9.7 g, 0.1 mol). After 1 h, triethyl borate (16.0 g, 0.11 mol) was added dropwise. The resulting mixture was stirred for 2 h, then allowed to warm to −30 °C, and treated with Me_3SiCl (15 mL, 0.12 mol). The mixture was allowed to warm to room temperature and then stirred for 1 h at 35−40 °C. The resulting suspension was filtered under argon. The filtrate was concentrated to leave a yellow oily residue. The product was obtained as a colorless liquid by distillation under reduced pressure. Bp: 90−94 °C (2 Tr). Yield: 15.4 g (78%). ^1H NMR (400 MHz, $CDCl_3$): δ 8.26−8.23 (m, 1H, py), 7.92−7.84 (m, 1H, py), 7.22−7.15 (m, 1H, py), 4.00 (t, J_{HH} = 7.2 Hz, 4H, OCH_2CH_3), 1.25 (t, J_{HH} = 7.2 Hz, 6H, OCH_2CH_3). ^{11}B NMR (64.16 MHz, $CDCl_3$): δ 28 ($w_{1/2}$ = 380 Hz).

*Synthesis of [py]$_2$B[Q] (**1**).* *n*-BuLi (1.0 mL, 0.01 mol) was added to a stirred solution of diisopropylamine (1.16 g, 0.01 mol) in THF (10 mL) at −78 °C. Then 2-fluoropyridine (1.11 g, 0.01 mol) was added. The resulting yellow suspension was stirred for 15 min followed by treatment with diethyl (2-fluoropyridin-3-yl)boronate (1.97 g, 0.01 mol). The reaction was allowed to warm to ca. 0 °C, and then 2 M HCl in Et_2O (5 mL, 0.01 mol) was added dropwise. The solution of 8-hydroxyquinoline H-Q (1.46 g, 0.01 mol) in THF (10 mL) was next added, and the mixture was finally quenched with H_2O (5 mL). The product was precipitated as a green solid. It was filtered, washed with H_2O (10 mL) and Et_2O (10 mL), and dried in a vacuum. Yield: 2.54 g (73%). Mp: 245−248 °C. ^1H NMR (400 MHz, DMSO-d_6): δ 9.03 (d, J = 5.2 Hz, 1H, Q), 8.87 (d, J = 8.4 Hz, 1H, Q), 8.11−8.10 (m, 2H, py), 7.97 (dd, J = 5.6 and 5.6 Hz, 1H, Q), 7.78−7.71 (m, 3H, Q + py),

dx.doi.org/10.1021/ic400729t | *Inorg. Chem.* 2013, 52, 10846−10859

7.50 (d, J = 8.4 Hz, 1H, Q), 7.25−7.22 (m, 3H, Q + py). ^{13}C NMR (100.6 MHz, DMSO-d_6): δ 165.5 (d, J_{CF} = 233 Hz, py), 156.9 (s, Q), 146.9 (d, J_{CF} = 15 Hz, py), 145.2 (d, J_{CF} = 10 Hz, py), 142.6 (d, J_{CF} = 6 Hz, py), 141.1 (s, Q), 136.4 (s, Q), 132.3 (s, Q), 128.0 (s, Q), 124.6 (s, Q), 121.7 (d, J_{CF} = 4 Hz, Q), 114.1 (s, Q), 109.4 (s, Q). ^{11}B NMR (64.16 MHz, acetone-d_6): δ 5 ($w_{1/2}$ = 900 Hz). Anal. Calcd for $C_{19}H_{12}BF_2N_3O$ (347.13): C, 65.74; H, 3.48; N, 12.11. Found: C, 65.41; H, 3.63; N, 12.08. DSC (second heating cycle): T_{g1} = 107.4 °C, T_{g2} = 187.8 °C, T_m = 253.2 °C. UV−vis (1.9×10^{-5} M in THF): λ_{max} = 381 nm, ε = 3800 M^{-1} cm^{-1}. Fluorescence: λ_{exc} = 381 nm, λ_{em} = 502 nm, Φ = 18%.

*Synthesis of [Ph][py]B[Q] (**2**).* *n*-BuLi (1.0 mL, 0.01 mol) was added to a stirred solution of bromobenzene (1.57 g, 0.01 mol) in THF/Et_2O (1:2, 15 mL) at −78 °C. After ca. 15 min, diethyl (2-fluoropyridin-3-yl)boronate (1.97 g, 0.01 mol) was added, and the mixture was stirred for 20 min, followed by quenching with 2 M aqueous HCl (5 mL, 0.01 mol). A solution of H-Q (1.46 g, 0.01 mol) in THF (10 mL) was added, and the crude product was precipitated. It was filtered, washed with H_2O (10 mL) and Et_2O (10 mL), and dried in a vacuum. Yield: 2.47 g (75%). Mp: 186−189 °C. ^{1}H NMR (400 MHz, DMSO-d_6): δ 9.11 (d, J = 5.0 Hz, 1H, Q), 8.81 (dd, J = 8.4 Hz, 1H, Q), 8.08−8.07 (m, 1H, py), 7.93 (dd, J = 8.4 and 5.0 Hz, 1H, Q), 7.80 (m, 1H, py), 7.70 (t, J = 8.4 Hz, 1H, Q), 7.45 (d, J = 8.4 Hz, 1H, Q), 7.35−7.33 (m, 2H, Ph), 7.25−7.15 (m, 5H, Q + py + Ph). ^{1}H NMR (400 MHz, $CDCl_3$): δ 8.86 (d, J = 5.2 Hz, 1H, Q), 8.44 (dd, J = 8.0 and 1.2 Hz, 1H, Q), 8.12−8.08 (m, 2H, py + Q), 7.69−7.65 (m, 2H, py + Q), 7.38 (dd, J = 8.0 and 1.5 Hz, 2H, Ph), 7.30−7.26 (m, 4H, Ph + Q), 7.19 (dd, J = 7.2 and 0.5 Hz, 1H, Q), 7.12 (m, 1H, py). ^{13}C NMR (100.6 MHz, DMSO-d_6): δ 165.8 (d, J_{CF} = 235 Hz, py), 157.3 (s, Q), 146.4 (d, J_{CF} = 15 Hz, py), 145.7 (d, J_{CF} = 9 Hz, py), 142.0 (d, J_{CF} = 5 Hz, py), 140.4 (s, Q), 136.4 (s, Q), 132.3 (s, Q), 131.0 (s, Ph), 128.0 (s, Q), 127.5 (s, Ph), 126.9 (s, Ph), 124.3 (s, Q), 121.4 (d, J_{CF} = 4 Hz, Q), 113.4 (s, Q), 109.0 (s, Q). ^{11}B NMR (64.16 MHz, DMSO-d_6): δ 11 ($w_{1/2}$ = 640 Hz). Anal. Calcd for $C_{20}H_{14}BFN_2O$ (328.15): C, 73.20; H, 4.30; N, 8.54. Found: C, 73.21; H, 4.33; N, 8.50. DSC (second heating cycle): T_c = 114.5 °C, T_m = 189.6 °C. UV−vis (1.8×10^{-5} M in THF): λ_{max} = 384 nm, ε = 4400 M^{-1} cm^{-1}. Fluorescence: λ_{exc} = 384 nm, λ_{em} = 503 nm, Φ = 20%.

*Synthesis of $ZnCl_2$·[**2**]$_2$ (**17**).* Compound **2** (440 mg, 1.34 mmol) was dissolved in CH_2Cl_2 (10 mL), and then $ZnCl_2$ (1 M solution in Et_2O, 0.67 mL, 0.67 mmol) was added with a syringe. The solution was filtered, and hexane (30 mL) was added to precipitate a pale-green solid. The mixture was stirred for 30 min, and the product was filtered and dried in vacuo. Mp: 211−213 °C. Yield: 420 mg (79%). ^{1}H NMR (400 MHz, $CDCl_3$): δ 8.66 (d, J = 4.8 Hz, 1H, Q), 8.48 (dd, J = 5.2 and 2.0 Hz, 1H, py), 8.42 (dd, J = 8.2 and 1.2 Hz, 1H, Q), 7.65 (dd, J = 8.4 and 7.6 Hz, 1H, Q), 7.59 (dd, J = 8.4 and 7.6 Hz, 1H, Q), 7.36−7.32 (m, 1H, py), 7.29 (m, 1H, Ar), 7.26 (m, 1H, Ar), 7.24 (m, 2H, Ph), 7.21−7.18 (m, 3H, Ph), 7.16 (m, 1H, Q). ^{13}C NMR (100.6 MHz, $CDCl_3$): δ 165.3 (d, J_{CF} = 249 Hz, py), 157.6 (s, Q), 150.2 (d, J_{CF} = 14 Hz, py), 146.1 (d, J_{CF} = 6 Hz, py), 141.0 (d, J_{CF} = 9 Hz, py), 139.7 (s, Q), 137.3 (s, Q), 132.6 (s, Q), 131.2 (s, Ph), 128.3 (s, Q), 127.9 (s, Ph), 127.6 (s, Ph), 123.3 (s, Q), 121.8 (d, J_{CF} = 2 Hz, Q), 113.3 (s, Q), 110.0 (s, Q). ^{11}B NMR (100.6 MHz, $CDCl_3$): δ 10 ($w_{1/2}$ = 580 Hz). Anal. Calcd for $C_{40}H_{28}B_2Cl_2F_2N_4O_2Zn{\cdot}H_2O$ (810.60): C, 59.27; H, 3.73; N, 6.91. Found: C, 59.19; H, 3.94; N, 6.97. UV−vis (5×10^{-6} M in CH_2Cl_2): λ_{max} = 389 nm, ε = 6700 M^{-1} cm^{-1}. Fluorescence: λ_{exc} = 389 nm, λ_{em} = 502 nm, Φ = 3%.

*Synthesis of {$ZnCl_2$[**1**]}$_2$ (**20**).* Compound **1** (350 mg, 1.00 mmol) was dissolved in CH_2Cl_2 (10 mL), and then $ZnCl_2$ (1 M solution in Et_2O, 1.00 mL, 1.00 mmol) was added with a syringe. A yellow solid precipitated after a few minutes. It was filtered, washed with CH_2Cl_2 (5 mL), and dried in vacuo. Its composition was determined by elemental analysis to be approximately $3ZnCl_2{\cdot}2$[**1**]. Yield: 0.35 g. Mp: >210 °C. This material was not completely soluble in $CDCl_3$. ^{1}H NMR (400 MHz, $CDCl_3$): δ 8.85 (d, J = 5.0 Hz, 1H, Q), 8.67 (d, J = 4.0 Hz, 2H, py), 8.61 (d, J = 8.0 Hz, 1H, Q), 7.91 (br, 2H, py), 7.86 (dd, J = 8.0 and 5.0 Hz, 1H, Q), 7.74 (t, J = 8.0 Hz, 1H, Q), 7.42 (d, J = 8.0 Hz, 1H, Q), 7.31 (t, J = 6.0 Hz, 2H, py), 7.25 (d, 1H, Q). A few single crystals of the complex **20** ($CDCl_3$ solvate) were grown by slow evaporation of the solution in the NMR tube.

Compounds **3**−**16** and **18**−**19** were synthesized according to the procedures described for compounds **2** and **17**, respectively. Details are given in the Supporting Information.

X-ray Data. Single-crystal X-ray measurements for compounds **1**, **3**, **4**, **10**, **17**, and **20** were performed on a Kuma KM4CCD k-axis diffractometer with graphite-monochromated Mo Kα radiation (λ = 0.71073 Å) and an Oxford Cryostream cooling device. Data reduction and analysis were carried out with the Oxford Diffraction Ltd. suite of programs.[68] Structures were solved by a direct method algorithm using *SHELXS*.[69] The IAM refinements, based on F^2, were performed with the *SHELXL*[69] program for all structures except of **10**. The structure of compound **10** was refined with the *CRYSTALS*[70] program. Weighted R factors (wR2) and all goodness-of-fit (GOF) values are based on F^2. Conventional R factors are based on F with F set to zero for negative F^2. The $F_o^2 > 2\sigma(F_o^2)$ criterion was used only for calculating R factors and is not relevant to the choice of reflections for the refinement. The R factors based on F^2 are about twice as large as those based on F. For structures of compounds **1**, **3**, **4**, **17**, and **20**, statistical weights were applied. For structure **10**, Chebychev (F^2) weights were applied. Atomic scattering factors, in their analytical form, were taken from the *International Tables for Crystallography*.[71] All non-hydrogen atoms were refined anisotropically, and all of the hydrogen atoms were placed in idealized positions (with 0.96 Å for C−H bond distances) within the riding model for atomic displacement parameters (ADPs) (with $U_{iso}^H = 1.2U_{eq}^C$). In all cases except the disordered Th ring in compounds **3**, hydrogen atoms were clearly visible on the residual density maps. In the case of **3**, the position of the Th ring was disordered and the refinement led to ca. 0.4:0.6 occupancies. Carefully chosen constraints were used to stabilize the crystallographic model. Because of the strong disorder present in the structure, we were unable to refine a more stable model with lower values of the residual densities.

In the case of **17**, the structure features a partial occupancy factor (50%) of the water molecule. This was also confirmed by calculations of the solvent-accessible volume performed with *PLATON*,[72] which show that the amount of void residual electron density corresponds to one solvent molecule per two molecules of the complex on average. In the case of **20**, the positions of $CDCl_3$ are characterized by different occupancy values. The C(39)DCl_3 molecule is ordered, and the position of this molecule is fully occupied. We suppose that this is due to the fact that this molecule forms quite short Cl···F and Cl···Cl intermolecular contacts [$d_{Cl(7)\cdots F(3)}$ = 3.151(6), 3.210(6), and 3.491(6) Å] and is stronger bonded to the structure. In contrast, the molecules C(40)DCl_3 (occupancy value equal to 0.35) and C(41)DCl_3 (occupancy value equal to 0.15) interact with the crystal framework very weakly and, therefore, are more likely to desorb from the structure. Large peaks of the residual electron densities (1.0−2.0 e $Å^{-3}$) were found near the C(41)DCl_3 molecule, which indicates disorder. It is also possible that other guest molecules (for example, acetone) were partially incorporated during crystal growth. However, we were not able to propose any reasonable model for this case. The unrefined density results in high R1 and wR2 parameter values. Hydrogen and deuterium atoms were included in the SFAC and UNIT instructions, but for both atoms, a hydrogen scattering factor number was employed. This procedure enables the formula weight and density to be correctly calculated. The CHECKCIF's alerts regarding the calculated chemical formula should not be taken into account. The *DIAMOND* program was used to generate crystal structures.[73] The CHECKCIF's "Alert B" for **3** is a consequence of identification of the sp^2 carbon atom as the sp^3 carbon atom by automatic algorithms implemented in the CHECKCIF program. CCDC 920413−920416, 950560, and 950561 contain the supplementary crystallographic data (CIF files) for this paper (for compounds **1**, **3**, **4**, **10**, **17**, and **20**, respectively). They can be obtained free of charge from the Cambridge Crystallographic Data Centre via www.ccdc.cam.ac.uk/data_request/cif or from the authors.

Optical Properties. UV−vis emission spectra were recorded using a Fluorolog 3-2-IHR320-TCSPC (from JobinYvon) spectrometer

equipped with a CCD detector calibrated with a Spectral Fluorescence Standard Kit[74] (certified by BAM Federal Institute for Materials Research and Testing). All emission data were obtained after excitation at the longest-wavelength absorption. The absorption spectra were recorded using a Shimadzu RF-5301 PC spectrometer. QYs of emission were determined using known procedures.[32] All measurements were carried out under room temperature. 9,10-Diphenylanthracene (DPA) was used as the standard for QY determination. The QY of DPA (ϕ_w) was adopted from Lakowicz.[32]

Electrochemical Properties. CV experiments were done in a three-electrode arrangement, with $Ag/AgNO_3$ (0.01 M) in acetonitrile as the reference electrode, platinum foil as the counter electrode, and glassy carbon as the working electrode. The reference electrode was separated from the working solution by an electrolytic bridge filled with the electrolyte solution 0.1 M tetrabutylammonium hexafluorophosphate/acetonitrile (Bu_4NPF_6/CH_3CN). The reference electrode potential was calibrated using a ferrocene electrode process in the same Bu_4NPF_6/CH_3CN solution [$E_0(FeCp_2^+/FeCp_2)$ = 0.087 V].

Differential Scanning Calorimetry (DSC) Measurements. DSC measurements were performed on a DSC Q200 calorimeter from TA Instruments. Melting points (T_m), glass transition temperatures (T_g), and crystallization temperatures (T_c) were calculated.

Theoretical Calculations. Geometry optimizations for **1**, **3**, **4**, and **10** were performed using their experimental X-ray geometries as the starting points at the RB3LYP/6-31+g(d,p) and UB3LYP/6-31+g(d,p) levels of theory. For other compounds, full optimizations were done. Orbital energies of the interacting molecules in the crystal structures of **1**, **3**, **4**, and **10** were calculated with the HF, RB3LYP, and B97D[75] levels of theory. In all cases, the C−H bond lengths were adjusted to standard neutron distances (1.083 Å)[76] prior to optimization/single-point calculations. Unrestricted DFT calculations were checked against spin contamination. For the iodine atom, the LANL2DZ effective core potential and the LANL2DZ basis set were used with additional d and f polarization functions according to a modification proposed by Glukhovtsev et al., with its complete-core relativistic effective core potential.[77] The obtained LANL2DZdf basis set in several tests proved to be more accurate than pure LANL2DZ.[78,79] Geometries of the excited states along with absorption and emission spectra were obtained using the TD-DFT method with the same basis set on the basis of the geometries obtained from ground-state optimizations. Subsequently, the vibrational frequencies were calculated, and the results showed that optimized geometries are stable structures. Tight-convergence criteria were used along with high-precision integrals (int=UltraFine) to obtain a good description of the boron coordination sphere. Wave functions were calculated without the use of symmetry constraints. All calculations were performed using the *Gaussian09*[80] suite of programs. The *VMD* program[81] was used for the visualization of molecular orbitals.

Charge-Transport Marcus theory. The charge-transport (CT) rate constant, k_{CT}, can be evaluated by eq 1:

$$k_{CT} = \frac{2\pi}{\hbar} H_{AB}{}^2 \frac{1}{\sqrt{4\pi\Lambda k_B T}} \exp\left[-\frac{(\Delta G^\circ + \Lambda)^2}{4\Lambda k_B T}\right] \quad (1)$$

where Λ is the reorganization energy, $H_{AB}{}^2$ is the electronic matrix element that represents the electronic coupling between donor and acceptor, T is the temperature, ΔG° is the standard free enthalpy, and k_B is the Boltzmann constant. The reorganization energy consists of two terms: the inner reorganization energy of the molecule, which is a fast process, and the reorganization energy of the surrounding medium, which is a slower process compared to the former one. In the condensed phase of an organic diode, the inner reorganization energy dominates, which can be confirmed by theoretical calculations. The inner reorganization energy for the hole transport (Λ_{hole}) is given by

$$\Lambda_{hole} = \Lambda_1 + \Lambda_+ = (E_0^{GS(+)} - E_0^{GS(0)}) + (E_+^{GS(0)} - E_+^{GS(+)}) \quad (2)$$

where $E_0^{GS(0)}$ and $E_+^{GS(0)}$ are the energies of the neutral and cationic states with the optimized geometry of the neutral species, respectively, while $E_0^{GS(+)}$ and $E_+^{GS(+)}$ are the energies of the neutral and cationic states with the optimized geometry of the cationic species. In the same manner, the inner reorganization energy for electron transport ($\Lambda_{electron}$) is evaluated by

$$\Lambda_{electron} = \Lambda_2 + \Lambda_- = (E_0^{GS(-)} - E_0^{GS(0)}) + (E_-^{GS(0)} - E_-^{GS(-)}) \quad (3)$$

Calculations of H_{AB} were carried out with Hartree−Fock (reference method), B3LYP, and B97D (more accurate potential with electron correlation and Grimm's dispersion correction). All calculations were done with the 6-31+g(d,p) basis set in *Gaussian09*. Contacts that may serve as pathways for charge hopping were chosen on the basis of their energies obtained using a semiempirical PIXEL method.[82−85] Detailed results of the analyzed paths are given in the Supporting Information (Tables S9−S28). All methods used gave qualitatively the same results. In all cases, there is no correlation between the energy of intermolecular contacts and the H_{AB} values. This may be rationalized by the fact that the strength of the interactions does not have to coincide with the effective overlap of the frontier orbitals.

■ ASSOCIATED CONTENT

Supporting Information

X-ray crystallographic data in CIF format for compounds **1**, **3**, **4**, **10**, **17**, and **20**, synthetic procedures and details of NMR characterization, X-ray crystallography, experimental optical properties, theoretical calculations, charge-transfer analysis of **1**, **3**, **4**, and **10**, and DSC characterization. This material is available free of charge via the Internet at http://pubs.acs.org.

■ AUTHOR INFORMATION

Corresponding Authors

*E-mail: grzegorz.wesela@chem.uw.edu.pl.
*E-mail: serek@ch.pw.edu.pl.

Notes

The authors declare no competing financial interest.

■ ACKNOWLEDGMENTS

The MPD/2010/4 project is realized within the MPD programme of Foundation for Polish Science, cofinanced from European Union, Regional Development Fund. This work was supported by the Polish Ministry of Science and Higher Education (Grant DEC-2011/03/B/ST5/02755). Support by Aldrich Chemical Co., Milwaukee, WI, through continuous donation of chemicals and equipment is gratefully acknowledged. G.W.-B. thanks the Foundation for Polish Science for financial support within the International Ph.D. Program. The authors gratefully acknowledge The Interdisciplinary Centre of Mathematical and Computational Modelling in Warsaw (Grant G33-14) for providing the computer facilities on which most of the calculations were done. Dr. Urszula Wawrzyniak from the Warsaw University of Technology is thanked for performing electrochemical measurements.

■ REFERENCES

(1) Rao, Y.-L.; Wang, S. *Inorg. Chem.* **2011**, *50*, 12263−12274.
(2) Tanaka, K.; Chujo, Y. *Macromol. Rapid Commun.* **2012**, *33*, 1235−1255.
(3) Nagai, A.; Chujo, Y. *Chem. Lett.* **2010**, *39*, 430−435.
(4) Jäkle, F. *Chem. Rev.* **2010**, *110*, 3985−4022.
(5) Entwistle, C. D.; Marder, T. B. *Chem. Mater.* **2004**, *16*, 4574−4585.
(6) Entwistle, C. D.; Marder, T. B. *Angew. Chem., Int. Ed.* **2002**, *41*, 2927−2931.
(7) Zhou, G.; Ho, C.-L.; Wong, W.-Y.; Wang, Q.; Ma, D.; Wang, L.; Lin, Z.; Marder, T. B.; Beeby, A. *Adv. Funct. Mater.* **2008**, *18*, 499−511.
(8) Letsinger, R. L.; Skoog, I. *J. Am. Chem. Soc.* **1955**, *77*, 2491−2494.

(9) Mitschke, U.; Bauerle, P. *J. Mater. Chem.* **2000**, *10*, 1471−1507.
(10) Popovic, Z. D.; Aziz, H.; Ioannidis, A.; Hu, N.-X.; dos Anjos, P. N. M. *Synth. Met.* **2001**, *123*, 179−181.
(11) Knox, J. E.; Halls, M. D.; Hratchian, H. P.; Bernhard Schlegel, H. *Phys. Chem. Chem. Phys.* **2006**, *8*, 1371−1377.
(12) Wu, Q.; Esteghamatian, M.; Hu, N.-X.; Popovic, Z.; Enright, G.; Breeze, S. R.; Wang, S. *Angew. Chem., Int. Ed.* **1999**, *38*, 985−988.
(13) Hassan, A.; Wang, S. *Chem. Commun.* **1998**, 211−212.
(14) Liu, W.; Hassan, A.; Wang, S. *Organometallics* **1997**, *16*, 4257−4259.
(15) Ashenhurst, J.; Brancaleon, L.; Hassan, A.; Liu, W.; Schmider, H.; Wang, S.; Wu, Q. *Organometallics* **1998**, *17*, 3186−3195.
(16) Wang, X.-Y.; Weck, M. *Macromolecules* **2005**, *38*, 7219−7224.
(17) Anderson, S.; Weaver, M. S.; Hudson, A. J. *Synth. Met.* **2000**, *111−112*, 459−463.
(18) Li, H.; Jäkle, F. *Angew. Chem., Int. Ed.* **2009**, *48*, 2313−2316.
(19) Tokoro, Y.; Nagai, A.; Chujo, Y. *Macromolecules* **2010**, *43*, 6229−6233.
(20) Nagata, Y.; Chujo, Y. *Macromolecules* **2007**, *40*, 6−8.
(21) Cui, Y.; Wang, S. *J. Org. Chem.* **2006**, *71*, 6485−6496.
(22) Nagata, Y.; Chujo, Y. *Macromolecules* **2008**, *41*, 2809−2813.
(23) Cui, Y.; Liu, Q.-D.; Bai, D.-R.; Jia, W.-L.; Tao, Y.; Wang, S. *Inorg. Chem.* **2005**, *44*, 601−609.
(24) Kappaun, S.; Rentenberger, S.; Pogantsch, A.; Zojer, E.; Mereiter, K.; Trimmel, G.; Saf, R.; Möller, K. C.; Stelzer, F.; Slugovc, C. *Chem. Mater.* **2006**, *18*, 3539−3547.
(25) Teng, Y. L.; Kan, Y. H.; Su, Z. M.; Liao, Y.; Yang, S. Y.; Wang, R. S. *Theor. Chem. Acc.* **2007**, *117*, 1−5.
(26) Qin, Y.; Kiburu, I.; Shah, S.; Jäkle, F. *Org. Lett.* **2006**, *8*, 5227−5230.
(27) Qin, Y.; Pagba, C.; Piotrowiak, P.; Jäkle, F. *J. Am. Chem. Soc.* **2004**, *126*, 7015−7018.
(28) Wu, Q.; Esteghamatian, M.; Hu, N.-X.; Popovic, Z.; Enright, G.; Tao, Y.; D'Iorio, M.; Wang, S. *Chem. Mater.* **2000**, *12*, 79−83.
(29) Wesela-Bauman, G.; Jastrzębski, L.; Kurach, P.; Luliński, S.; Serwatowski, J.; Woźniak, K. *J. Organomet. Chem.* **2012**, *711*, 1−9.
(30) Sakanoue, K.; Motoda, M.; Sugimoto, M.; Sakaki, S. *J. Phys. Chem. A* **1999**, *103*, 5551−5556.
(31) Shirota, Y.; Kageyama, H. *Chem. Rev.* **2007**, *107*, 953−1010.
(32) Lakowicz, J. R. *Principles of Fluorescence Spectroscopy*; 2nd ed.; Kluwer Academic/Plenum Publishers: Amsterdam, The Netherlands, 1999.
(33) Hou, C.; Zhao, Y.; Lu, Y.; Wang, P.; Sun, W.-Y. *Inorg. Chem. Commun.* **2012**, *20*, 317−321.
(34) Yu, F.; Yu, W.-J.; Li, B.; Zhang, T.-L. *CrystEngComm* **2012**, *14*, 6770−6777.
(35) Wu, H.-L.; Yuan, J.-K.; Huang, X.-C.; Kou, F.; Liu, B.; Jia, F.; Wang, K.-T.; Bai, Y. *Inorg. Chim. Acta* **2012**, *390*, 12−21.
(36) Guo, Y.; Ma, P.; Wang, J.; Niu, J. *J. Solid State Chem.* **2011**, *184*, 3121−3127.
(37) Arbuzova, S. N.; Volkov, P. A.; Ivanova, N. I.; Gusarova, N. K.; Larina, L. I.; Kazheva, O. N.; Alexandrov, G. G.; Dyachenko, O. A.; Trofimov, B. A. *J. Organomet. Chem.* **2011**, *696*, 2053−2058.
(38) Hoanh, T. D.; Im, Y. H.; Kim, D.-E.; Kwon, Y.-S.; Lee, B.-J. *J. Nanomater.* **2012**.
(39) Xiao, X.; He, Y.; Sun, L.; Wang, G.; Shen, L.; Fang, J.; Gao, H.; Yang, J. *Transition Met. Chem.* **2012**, *37*, 771−775.
(40) Ojwach, S. O.; Nyamato, G. S.; Omondi, B.; Darkwa, J. *Inorg. Chim. Acta* **2012**, *392*, 141−147.
(41) Qin, S.; Huang, H.; Chen, Z.; Liang, F. *Struct. Chem.* **2011**, *22*, 559−565.
(42) Cheng, F.; Bonder, E. M.; Salem, S.; Jäkle, F. *Macromolecules* **2013**, *46*, 2905−2915.
(43) Höpfl, H. *J. Organomet. Chem.* **1999**, *581*, 129−149.
(44) Spackman, M. A.; McKinnon, J. J. *CrystEngComm* **2002**, *4*, 378−392.
(45) McKinnon, J. J.; Spackman, M. A.; Mitchell, A. S. *Acta Crystallogr., Sect. B* **2004**, *60*, 627−668.
(46) McKinnon, J. J.; Jayatilaka, D.; Spackman, M. A. *Chem. Commun.* **2007**, *0*, 3814−3816.
(47) Spackman, M. A.; Jayatilaka, D. *CrystEngComm* **2009**, *11*, 19−32.
(48) Ivanova, B.; Spiteller, M. *Polyhedron* **2011**, *30*, 241−245.
(49) Liu, Y.-H.; Xu, L.; Dai, D.-M.; Zou, J.-W. *Acta Crystallogr., Sect. E* **2011**, *67*, m915.
(50) Li, Y.; Liu, Z.; Deng, H. *Acta Crystallogr., Sect. E* **2007**, *63*, m3065.
(51) İde, S.; Ataç, A.; Yurdakul, Ş. *J. Mol. Struct.* **2002**, *605*, 103−107.
(52) Wang, R.; Dols, T. S.; Lehmann, C. W.; Englert, U. *Chem. Commun.* **2012**, *48*, 6830−6832.
(53) Adarsh, N. N.; Dastidar, P. *Cryst. Growth Des.* **2011**, *11*, 328−336.
(54) Zhang, X.; Zhou, X.-P.; Li, D. *Cryst. Growth Des.* **2006**, *6*, 1440−1444.
(55) Xia, Y.; Li, S.; Wu, B.; Liu, Y.; Yang, X.-J. *CrystEngComm* **2011**, *13*, 5763−5772.
(56) Liang, J.; Wu, B.; Jia, C.; Yang, X.-J. *CrystEngComm* **2009**, *11*, 975−977.
(57) Jia, T.; Zhao, Y.; Xing, F.; Shao, M.; Zhu, S.; Li, M. *J. Mol. Struct.* **2009**, *920*, 18−22.
(58) Wang, R.; Han, L.; Xu, L.; Gong, Y.; Zhou, Y.; Hong, M.; Chan, A. S. C. *Eur. J. Inorg. Chem.* **2004**, *2004*, 3751−3763.
(59) Stone, K. G.; Friedman, L. *J. Am. Chem. Soc.* **1947**, *69*, 209−211.
(60) Hellstrom, S. L.; Ugolotti, J.; Britovsek, G. J. P.; Jones, T. S.; White, A. J. P. *New J. Chem.* **2008**, *32*, 1379−1387.
(61) Becke, A. D. *Phys. Rev.* **1988**, *38*, 3098−3100.
(62) Lee, C.; Yang, W.; Parr, R. G. *Phys. Rev. B* **1988**, *37*, 785−789.
(63) Krishnan, R.; Binkley, J. S.; Seeger, R.; Pople, J. A. *J. Chem. Phys.* **1980**, *72*, 650−654.
(64) Marcus, R. A.; Sutin, N. *Biochim. Biophys. Acta, Rev. Bioenerg.* **1985**, *811*, 265−322.
(65) Lin, B. C.; Cheng, C. P.; You, Z.-Q.; Hsu, C.-P. *J. Am. Chem. Soc.* **2005**, *127*, 66−67.
(66) Li, X.-N.; Feng, J.-K.; Ren, A.-M. *Chin. J. Chem.* **2008**, *26*, 1979−1984.
(67) Lan, Y.-K.; Huang, C.-I. *J. Phys. Chem. B* **2008**, *112*, 14857−14862.
(68) *CrysAlis Pro Software*; Oxford Diffraction Ltd.: Oxford, U.K., 2010.
(69) Sheldrick, G. M. *Acta Crystallogr.* **2008**, *64*, 112−122.
(70) Betteridge, P. W.; Carruthers, J. R.; Cooper, R. I.; Prout, K.; Watkin, D. J. *J. Appl. Crystallogr.* **2003**, *36*, 1487.
(71) Fuess, H., Ed. *International Tables for Crystallography,Mathematical, Physical and Chemical Tables*; Kluwer Academic Publishers: Chester, U.K., 2006; Vol. *C*.
(72) Spek A. L. *PLATON, A Multipurpose Crystallographic Tool*; Utrecht University: Utrecht, The Netherlands, 2001.
(73) Putz, H.; Brandenburg, K. *DIAMOND—Crystal and Molecular Structure Visualization*; Crystal Impact GbR: Bonn, Germany, 2012.
(74) Pfeifer, D.; Hoffmann, K.; Hoffmann, A.; Monte, C.; Resch-Genger, U. *J. Fluoresc.* **2006**, *16*, 581−587.
(75) Grimme, S. *J. Comput. Chem.* **2006**, *27*, 1787−1799.
(76) Allen, F. H.; Bruno, I. J. *Acta Crystallogr., Sect. B* **2010**, *66*, 380−386.
(77) Glukhovtsev, M. N.; Pross, A.; McGrath, M. P.; Radom, L. *J. Chem. Phys.* **1995**, *103*, 1878−1885.
(78) East, A. L. L.; Berner, G. M.; Morcom, A. D.; Mihichuk, L. *J. Chem. Theory Comput.* **2008**, *4*, 1274−1282.
(79) Hepperle, S. S.; Li, Q.; East, A. L. L. *J. Phys. Chem. A* **2005**, *109*, 10975−10981.
(80) Frisch, M. J.; Trucks, G. W.; Schlegel, H. B.; Scuseria, G. E.; Robb, M. A.; Cheeseman, J. R.; Scalmani, G.; Barone, V.; Mennucci, B.; Petersson, G. A.; Nakatsuji, H.; Caricato, M.; Li, X.; Hratchian, H. P.; Izmaylov, A. F.; Bloino, J.; Zheng, G.; Sonnenberg, J. L.; Hada, M.; Ehara, M.; Toyota, K.; Fukuda, R.; Hasegawa, J.; Ishida, M.; Nakajima, T.; Honda, Y.; Kitao, O.; Nakai, H.; Vreven, T.; Montgomery, J. A., Jr.; Peralta, J. E.; Ogliaro, F.; Bearpark, M.; Heyd, J. J.; Brothers, E.; Kudin,

K. N.; Staroverov, V. N.; Keith, T.; Kobayashi, R.; Normand, J.; Raghavachari, K.; Rendell, A.; Burant, J. C.; Iyengar, S. S.; Tomasi, J.; Cossi, M.; Rega, N.; Millam, J. M.; Klene, M.; Knox, J. E.; Cross, J. B.; Bakken, V.; Adamo, C.; Jaramillo, J.; Gomperts, R.; Stratmann, R. E.; Yazyev, O.; Austin, A. J.; Cammi, R.; Pomelli, C.; Ochterski, J. W.; Martin, R. L.; Morokuma, K.; Zakrzewski, V. G.; Voth, G. A.; Salvador, P.; Dannenberg, J. J.; Dapprich, S.; Daniels, A. D.; Farkas, O.; Foresman, J. B.; Ortiz, J. V.; Cioslowski, J.; Fox, D. J. *Gaussian09*; Gaussian, Inc.: Wallingford, CT, 2010.

(81) Humphrey, W.; Dalke, A.; Schulten, K. *J. Mol. Graph.* **1996**, *14*, 33−38.

(82) Gavezzotti, A. *J. Phys. Chem. B* **2003**, *107*, 2344−2353.

(83) Gavezzotti, A. *J. Phys. Chem. B* **2002**, *106*, 4145−4154.

(84) Gavezzotti, A. *J. Chem. Theory Comput.* **2005**, *1*, 834−840.

(85) Gavezzotti, A. *CrystEngComm* **2003**, *5*, 429−438.